

Development of Detailed AF05%ile Hybrid III Dummy FE Model

Tsuyoshi Yasuki

Toyota

*This paper has not been screened for accuracy nor refereed by any body of scientific peers
and should not be referenced in the open literature.*

ABSTRACT

This paper describes a development of Hybrid III AF05%ile dummy FE model by reverse engineering. Better fidelities of the FE models of Anthropomorphic Test Dummy (ATD) are regarded to depend on more accurate geometry, material properties and joint stiffness of the FE models of the ATDs. In this research, geometries of Hybrid III AF05%ile dummy were measured using X-ray CT scans. Material properties of components of the dummy were measured by static and dynamic coupon tests. Joint stiffness of the dummy was measured by tests. An FE model of Hybrid III AF05%ile dummy was generated from scratch by referring these geometries, material properties and joint stiffness. Sled impact test simulation was conducted by the FE model. Kinematics and injury index values by the FE model indicated good correlations with those of sled impact test.

INTRODUCTION

Efforts have been performed for improving fidelities of the FE models of Anthropomorphic Test Dummies (ATDs). Moss et al. developed an FE model of AM50%ile Hybrid III crash test dummy (Moss et al., 1997), Mohan et al. developed an FE model for the AF05%ile Hybrid III crash test dummy (Mohan et al., 2009), and Shirooka et al. clarified mechanisms of chest acceleration during frontal crash test by FE model of AM50%ile Hybrid III crash test dummy (Shirooka et al., 2008). However, better fidelities of the FE models of ATDs are still regarded to depend on more accurate geometry, material properties and joint stiffness of the FE models of the ATDs.

This paper describes improving the fidelities of FE model of AF05%ile Hybrid III crash test dummy (Figure 1) by reverse engineering of geometries, material properties and joint stiffness. X-ray computed tomography (CT) scans were used to measure both the external geometry and internal structure of the dummy in this research and geometry of the dummy was reproduced as grid points in STL format. The mechanical properties of the dummy component parts and the stiffness of each joint were measured and then applied these properties into the FE model. Characteristics of force-displacement curves of the FE model were compared to the experimental data to validate fidelities of the dummy FE model. This dummy FE model was installed to a sled FE model and used to analyze the dummy injury mechanisms in frontal impact sled test and fidelities of the dummy FE model proved to be good.

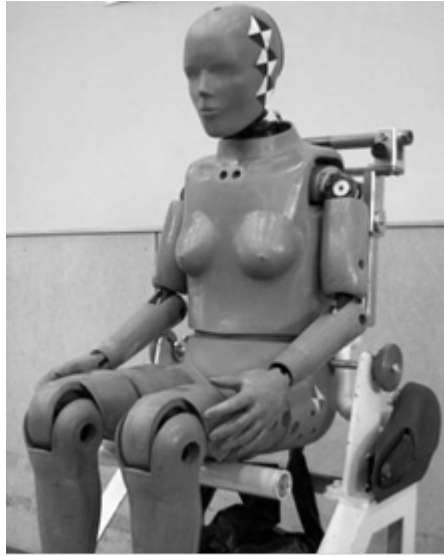


Figure 1: AF05%ile Hybrid-III Dummy

METHODS

Geometry

X-ray CT scan system used to measure the geometry of the dummy component parts as three dimensional (3D) data in an assembled condition (Okada et al., 2003). The scan system generated a lot of 2 dimensional (2D) image slices, while the images were obtained with a pitch of 1.0 mm and a pixel size of 0.4 mm (Figure 2). Finite element of the dummy was generated using shell and solid elements (Figure 3) by using three dimensional data of the geometry of the dummy component parts. Size of shell elements and solid elements were from 3 to 10 mm. The FE model consisted of 336 parts and 253,000 elements (Table 1). The mass and center of gravity of each component of the FE model was set based on the values referenced from the National Highway Traffic Safety Administration (NHTSA) in the U.S. (Table 2).

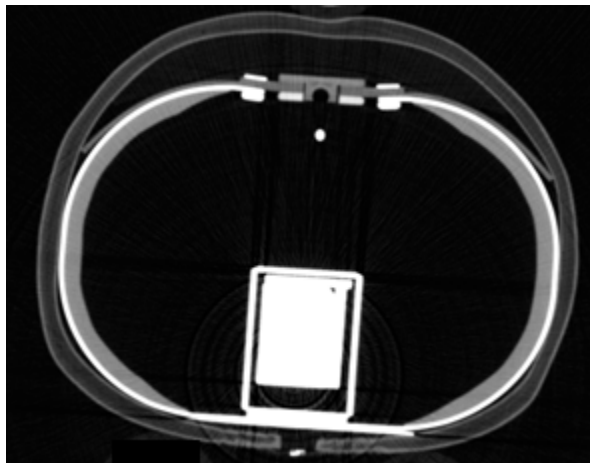
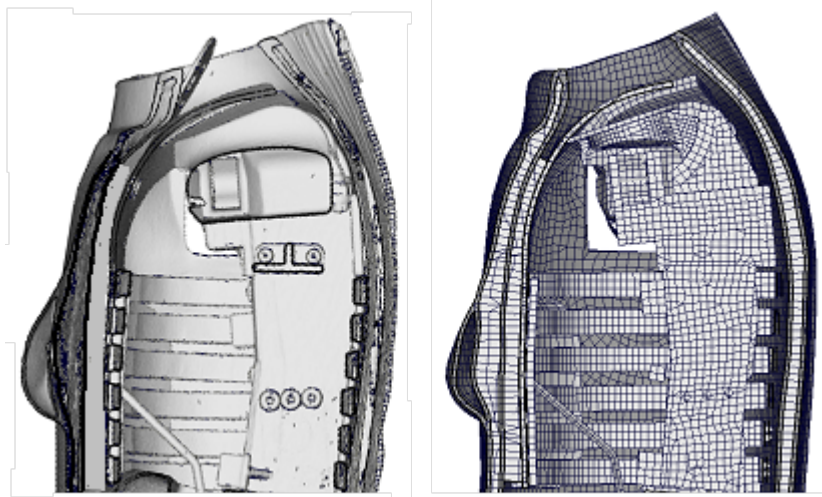


Figure 2: 2D images slices of thorax by CT



(a) Scanned Data by CT (b) FE Model
 Figure 3: Comparison of Thorax Section

Table 1: The Number of parts, nodes and Elements of the FE Model

TYPE	NUMBER
Part	336
Node	293712
Solid	253577
Shell	230282
Beam	88

Table 2: Comparison of Mass of Assembly of parts

ASSEMBLY	MEASURED MASS [KG]	MASS OF FE MODEL [KG]
Head	3.37	3.74
Neck	0.91	0.89
Upper torso	12.02	11.96
Lower torso	13.24	13.32
Upper arm	2.36	2.38
Lower arm and hands	2.36	2.32
Upper legs	6.26	6.23
Lower legs and feet	8.12	8.13
Total	49	48.97

Material Properties

Materials parts such as steel used for skeletal parts, vinyl or urethane used for the dummy skin, and rubber used for the neck, lumbar spine, deform during frontal sled tests. Accurate material properties are necessary for FE model of ATD to reproduce similar deformation of each part to those of AF05%ile Hybrid-III dummy. Material properties of 49 materials of the dummy were measured in static tension or compression coupon tests (Table 3). Dynamic mechanical properties were measured for 7 materials to identify strain rate dependency of material constitutive laws.

The measurement was performed using a Tensilon UCT-1T universal tester. The static tensile test was performed at 0.8 mm/s and the dynamic tensile test was performed at 10 m/s. The test specimens were prepared by analyzing a new physical dummy and cutting out material with the required length for measurement. Figure 4 shows an example of an extracted test specimen. The force and deformation properties from the measured data was recorded and used to extract the necessary parameters for the material model.

Table 3: The number of Test Specimens

MATERIAL TYPE	THE NUMBER OF SPEICMENS
Steel	26
Aluminum	5
Dumping material	2
Rubber	8
Vinyl	5
Ensolite	1
Others	2

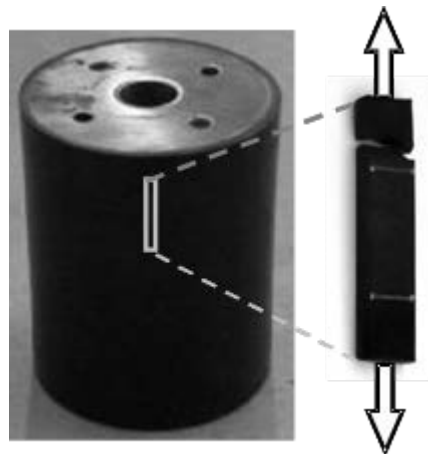


Figure 4: Lumber spine and test specimens after coupon test

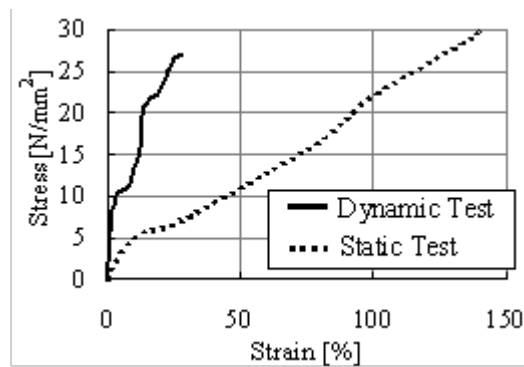


Figure 5: Relation between stress and strain of lumber spine

Joint Stiffness

AF05%ile Hybrid III crash test dummy has 27 rotational joints. Joint torque of the dummy and its rotation angle limits of the rotational joints were measured. The joint torque was measured using a push-pull gauge generating the reaction force when the overall center of gravity of the movable portion was pulled up as shown in Figure 6. The joint torque value was calculated by multiplying the measured reaction force by the distance from the joint to the center of gravity. The rotation angle limits were also calculated. The average of 15 data obtained from 5 dummies that were measured 3 times each was used in this research.



Figure 6: Measurement of joint stiffness

VALIDATION

The FE model was validated to the standard certification tests recommended in the Code of Federal Regulations under 49 CFR Part 572 (Part 577).

Head Drop Test

Figure 7 shows the verification FE model used in the head drop test. Aluminum skull was modeled as solid elements. The material type 77 of LS-DYNA (Ogden_rubber) was used to model the skin. In compliance with the Part 572 standard, the FE head model was dropped from a height of 376 mm onto a 50.8 mm thick steel plate with nodes constrained in 6 degrees of freedom (DOF). The obtained deceleration waveform was run through an SAE class 1000 filter. The time-history comparison for the drop test and simulation are shown in Figure 8. The deceleration results using the FE model are consistent with those from the test. Peak value and timing are consistent with the test. The maximum resultant deceleration fits the predefined response corridor.

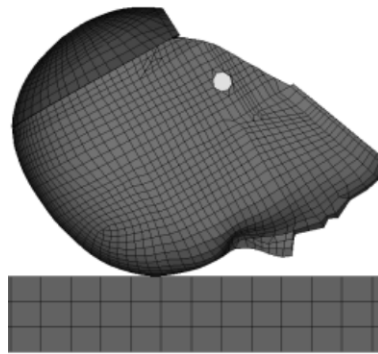


Figure 7: Head drop test

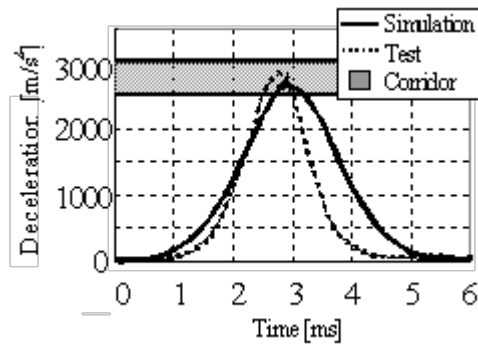


Figure 8: Comparison of deceleration of head

Neck Extension and Flexion Test

Figure 9 shows the verification FE model used in the neck pendulum test. The 5 metal discs comprising the neck were modeled using shell elements designated as elastic element. The rubber between the discs was modeled as solid elements using the material type 77 of LS-DYNA (Ogden_rubber). The holes and slits of the neck in the dummy were also expressed. The pendulum with a length of 1,867 mm and a mass of 29.57 kg was modeled as elastic shell element. The pendulum side and dummy neck lower bracket were joined to ensure the same rotational movement. The obtained waveform was run through an SAE class 1000 filter. The time-history of the rotation angle comparison for the test and simulation are shown in Figure 10. The simulation results show good correlation with the test result. It was confirmed that the maximum rotation angle and the time of intersection with the 10 Nm point fits the predefined response corridor. It was also confirmed that the resultant moment was within the corridor.

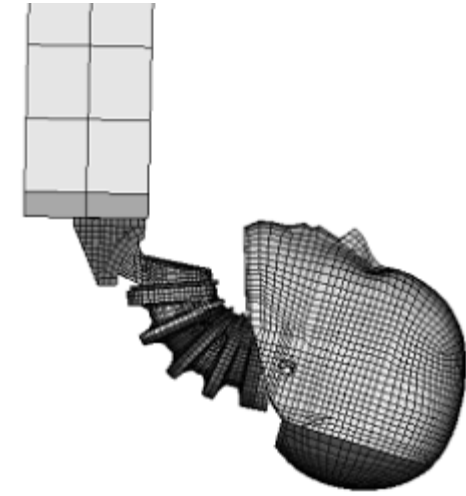


Figure 9: Neck pendulum test

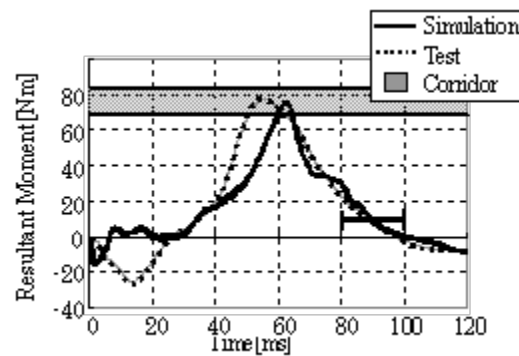


Figure 10: Comparison of Rotation Angle

Rib Impact Test

Since ribs play a major role in frontal impact for generating reaction force among the parts comprising the chest, a verification test was conducted using a single rib from the thorax before carrying out the thorax impact test. In the FE rib model, the thin outer metal sheets of the rib were modeled as elastic shell elements, and the inner mass damper portion was modeled as solid elements. The spine box was also modeled as elastic solid elements. For the rib impact test, this development applied original static horizontal load test on a dummy rib and then compared with simulation. In the test, the spine box was constrained to the jig by a bolt. The rib impacted with the impactor at 20 mm/min. In the simulation, the spine box node was constrained in 6 DOF. A plate comprising a metal sheet and a buffer modeled from foam material were combined to the front of the rib. The rib impacted with the impactor at 0.1 m/s in the same way as in the test (Figure 11). Figure 12 compares the results from the simulation and test. The simulation results show good correlation to the test.

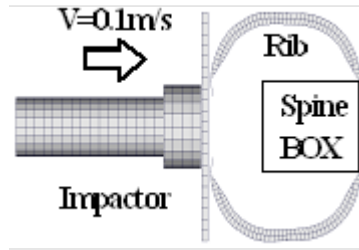


Figure 11: Rib Impact Test

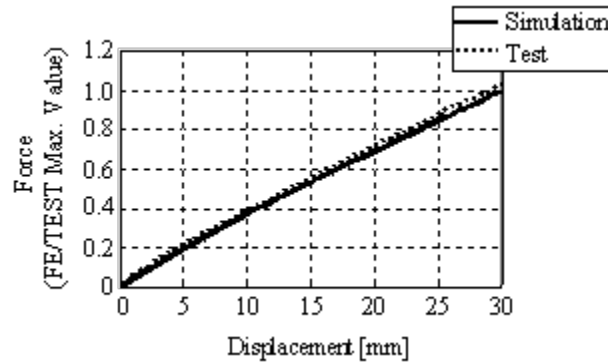


Figure 12: Comparison of Rib Force

Thorax Impact Test

Figure 13 shows the FE model used in the thorax impact test. In addition to the ribs and spine structured as described above, the thorax also consists of a jacket, bib, sternum, and other parts. The material type 77 was used to model the jacket skin. The material type 57 (Low density foam) was used to model the jacket inner urethane. A volumetric strain-dependent viscoelastic model was adopted for the bib to ensure accuracy under compressive force. The parts were joined by beam, rigid, and joint elements. The FE dummy was seated on a rigid surface and impacted by a pendulum with a mass of 13.97 kg at 6.7 m/s. Furthermore, original verification test was also carried out at 2.7 m/s, equivalent to the deformation rate of the thorax surface in a 56 km/h frontal crash. The obtained results were run through an SAE class 180 filter. Figure 14 compares the chest deflection waveforms from the simulation and the test. Although the maximum value is within the corridor at initial speed of 6.7 m/s, the difference is observed in the transitional characteristics between the simulation and the test. However, both the maximum value and the transitional characteristics of the simulation results are good correlation to the test at 2.7 m/s. The results indicate that the FE model could be used for the impact analysis.

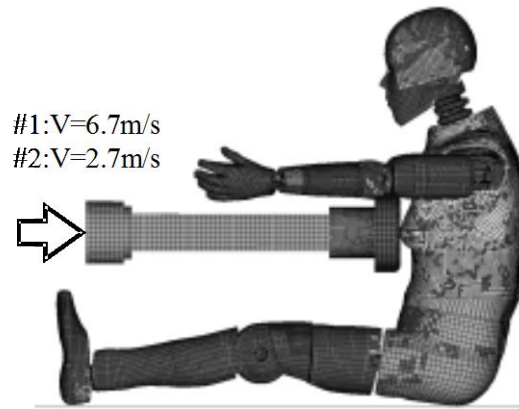


Figure 13: Thorax Impact Test (FE Model)

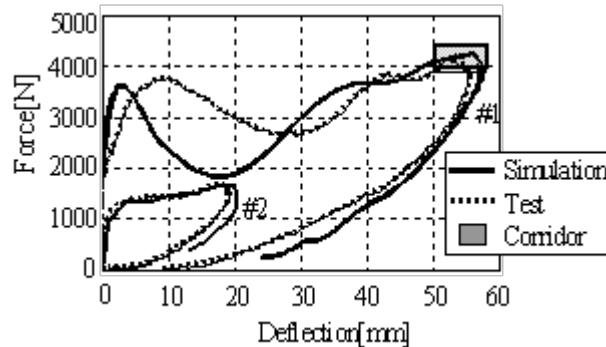


Figure 14: Comparison of Chest Deflection

Torso Flexion Test

Figure 15 shows the FE model used in the torso flexion test. The lower torso is the most complex assembly in the dummy. The main parts in the lower torso are as follows: lumbar spine, lumbar spine mount, aluminum girdle, outer vinyl, inner foam, and abdomen. The lumbar spine was modeled as solid elements, and assigned material type 77 of LS-DYNA. The lumbar spine was connected to the spine box and the lumbar spine mount using the nodal rigid body. The wire rope used in the lumbar spine was modeled as beam elements. The pelvis, lumbar spine mount and inner foam were modeled as solid elements. The inner form was assigned material type of FU CHANG FOAM of LS-DYNA. The material type 77 was used to model the outer vinyl. Finally, the abdomen was modeled as solid elements. The material type 77 was used to the abdominal skin, and the internal abdomen was modeled as airbag defining stiffness. A rigid jig attached to the upper spine of the seated dummy on the rigid table was connected with cable to the pulley on the table. Apply a tension force in the midsagittal plane to the pull cable at 57.3rad/s. FE simulation was conducted based on the test procedure outlined in the 49 CFR Part 572. The obtained data were run through an SAE class 180 filter. The torso flexion angle versus pulling force curves comparing between the test and simulation result are shown in Figure 16. The Figure shows good correlation between the test and simulation result. It was confirmed that the force at 45 degrees in the flexion was within the corridor.

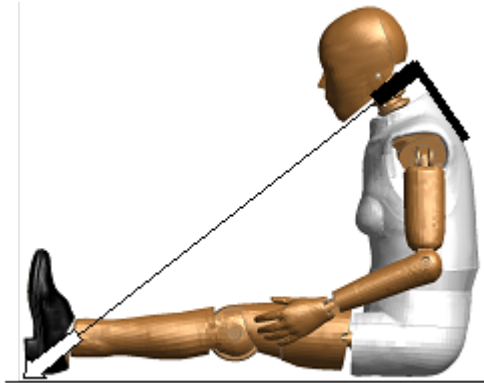


Figure 15: Torso Flexion Test (FE Model)

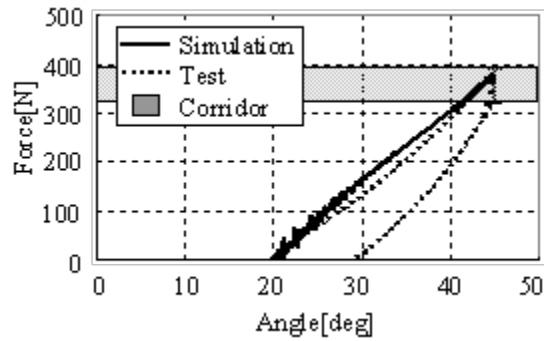


Figure 16: Comparison of Pulling Force

Sled test

Figure 17 shows the sled FE model that was used in the validation calculation. The sled model was based on the model developed by Shirooka et al (Shirooka et al., 2008). The components that affect the kinematics of the dummy, such as instrumental panel, airbag, seatbelt, seat foam, were modeled. The dummy FE model was placed in the front passenger seat of the sled model and applied a 35 mph sled pulse. The first half of the simulation was used to seat the dummy in the target position. After reproducing the reaction force from the seat directly before the crash, the deceleration generated during a crash test was then applied to the sled body.



Figure 17: Sled FE Model

Comparison of the dummy kinematics between the sled test and the simulation at the timing of maximum chest deceleration (70 ms) is shown in Figure 18. As examples of injury criteria, the time-history of chest deceleration comparison for test and simulation are shown in Figure 19. The simulated dummy kinematics and maximum values of chest deceleration well coincide with the test results.



Figure 18: Comparison of Sled Test Kinematics (70 ms)

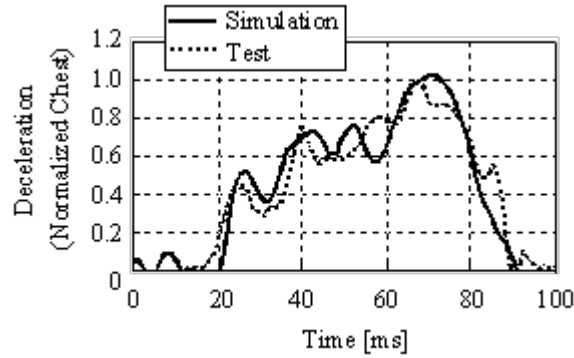


Figure 19: Comparison of Chest Deceleration at the Sled Test

RESULTS AND DISCUSSION

Results

Figure 20 shows the time-history of chest deceleration and seatbelt shoulder force. Chest deceleration begins to rise up at 20ms with the seatbelt pretensioner on. Then, the chest deceleration starts to increase, while the shoulder seatbelt force keeps shoulder and upper ribs are controlled by the load limiter, meanwhile, the force on the lower chest is rising up with the torso forward. The results show that the applied force to the lower chest transmitted to the spine box through the rib induced the increase of the chest deceleration.

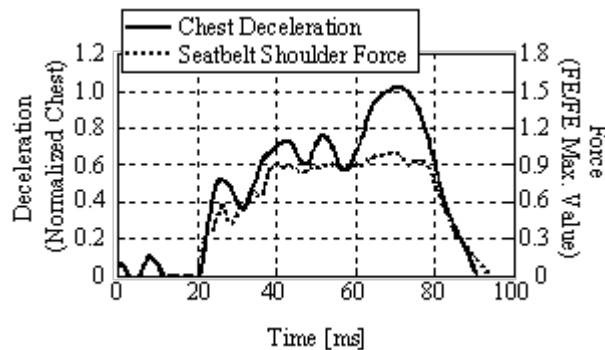


Figure 20: Comparison of Chest Deceleration and Seatbelt shoulder Force

Discussion

Figure 20 shows the time-history of chest deceleration and seatbelt shoulder force. Chest deceleration begins to rise up at 20ms with the seatbelt pretensioner on. Then, the chest deceleration starts to increase, while the shoulder seatbelt force keeps constant from 38ms with the load limiter. This phenomenon was analyzed using the FE model. Figure 21 and 22 show stress concentrates upon the upper thorax loaded by the seatbelt force at 38ms of the start timing of load limiter and at 70ms of the timing of maximum chest deceleration respectively. Comparing the stress contour between the two timings, the shoulder and the stress in the 1st rib to the 5th keeps low level, while the 6th rib is increasing. The result indicates that the force loaded on the shoulder and upper ribs are controlled by the load limiter, meanwhile, the force on the lower chest is rising up with the torso forward. The results show that the applied force to the lower chest transmitted to the spine box through the rib induced the increase of the chest deceleration.

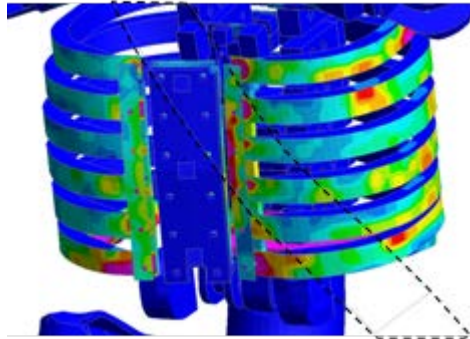


Figure 21: Contour of von Mises Stress (38ms)

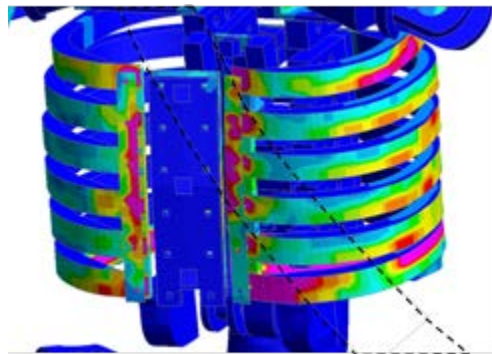


Figure 22: Contour of von Mises Stress (70ms)

CONCLUSIONS

The detail geometry of the assembled dummy was measured using X-ray CT, and from the data, the FE model of the AF05%ile Hybrid III dummy was modeled. Material properties were optimized by cutting out test specimens from dummy component parts and performing static and dynamic tests. The identified material properties were assigned to the FE model. The developed detail FE model showed reasonable correlation for head drop, neck extension and flexion, thorax impact, torso flexion tests. It was concluded that the FE model was effective for analyzing the internal deformation and load transfer during the crash test.

ACKNOWLEDGEMENTS

We would like to acknowledge Mr. Yoichiro Ohnishi, Miss Mariko Honda, Mr. Hayato Kaneko and Mr. Tatsuya Komamura at Toyota Motor Corporation for providing research support.

REFERENCES

- MOHAN, P., MARZOUGUI, D., KAN, C. D. (2009). Development and Validation of Hybrid III Crash Test Dummy, SAE Paper 2009-01-0473.
- MOSS, S., HUANG, Y., KEER, T. and SHAH, B. (1997), Development of an Advanced Finite Element Model Database of the Hybrid III Crash Test Dummy Family. SAE Paper, No. 971042.
- OKADA, T. MIWATA, Y. and ISHII, H. (2003). Three-Dimensional Shape Measurement With High-Energy X-Ray CT-Scan, SAE Paper No. 2003-01-1033.
- SIROOKA, M., KOMAMURA, T., KUMAGAI, K. and YASUKI, T. (2008). Reduction of unevenness in occupant injury index on passenger side in frontal collision. JSAE Transaction, Vol.39, No.6, 20086031.